

THE INFORMATION DYNAMICS OF GENERATIVE DIFFUSION

Luca Ambrogioni

Donders Institute for Brain, Cognition and Behaviour
Radboud University
luca.ambrogioni@donders.ru.nl

ABSTRACT

Generative diffusion models have emerged as a powerful class of models in machine learning, yet a unified theoretical understanding of their operation is still developing. This paper provides an integrated perspective on generative diffusion by connecting their dynamic, information-theoretic, and thermodynamic properties under a unified mathematical framework. We demonstrate that the rate of conditional entropy production during generation (i.e. the generative bandwidth) is directly governed by the expected divergence of the score function's vector field. This divergence, in turn, is linked to the branching of trajectories and generative bifurcations, which we characterize as symmetry-breaking phase transitions in the energy landscape. This synthesis offers a powerful insight: the process of generation is fundamentally driven by the controlled, noise-induced breaking of (approximate) symmetries, where peaks in information transfer correspond to critical transitions between possible outcomes. The score function acts as a dynamic non-linear filter that regulates the bandwidth of the noise by suppressing fluctuations that are incompatible with the data.

1 INTRODUCTION

In this paper, we outline a conceptual perspective on generative diffusion models. Our goal is to provide a connection between the dynamic, the thermodynamic and the information theoretical aspects by showing that entropy production (information theory) is directly related to the branching of trajectories (dynamics), which in turn is a consequence of symmetry-breaking phase-transitions in the potential energy (thermodynamics). While we will present several original derivations, the aim of this paper is not to provide new mathematical results but to provide an integrated picture of the information theory and statistical physics of generative diffusion.

2 RELATED WORK

This paper integrates insights coming from a multitude of sources. Diffusion models were introduced in (Sohl-Dickstein et al., 2015) in analogy with non-equilibrium thermodynamics. Several following works elucidated the theoretical foundations of the method (Song et al., 2021; Ho et al., 2020; Song et al., 2022) and their practical implementation procedures Ho et al. (2020); Dhariwal & Nichol (2021). The mathematical framework used here based on stochastic differential equations (SDEs) was formulated in (Song et al., 2021; Rombach et al., 2022) and is central to the modern understanding of diffusion models.

The connections between statistical physics and generative diffusion have been heavily studied in the past few years. Recent works on stochastic localization highlighted direct formal connections with generative diffusion process (Alaoui et al., 2023; Huang et al., 2024), which can be extended to an elegant general framework for sampling (Montanari, 2023; Benton et al., 2024; Alaoui et al., 2023). Concerning the link between generative diffusion and phase transitions, notable developments were the characterizations of high dimensional limits (Biroli & Mézard, 2023) and the identification of mean-field spontaneous symmetry breaking events in the generative dynamics, corresponding to

generative bifurcations (Raya & Ambrogioni, 2023; Ambrogioni, 2024b). Using hierarchical generative models, Sclocchi et al. (2025b) identified phase transitions at different hierarchical levels corresponding to the emergence of semantic features during generation. The analysis was later refined in (Sclocchi et al., 2025a), where the authors analyzed the emergence of power law scaling in the statistics of the generated samples. Generative bifurcation and memorization transitions were further studied in (Biroli et al., 2024) and the analysis was later refined in (Bonnaire et al., 2025; Achilli et al., 2025; 2024). Generative diffusion models have also been directly connected to modern Hopfield networks and other associative memory networks Ambrogioni (2024a); Hoover et al. (2023); Hess & Morris (2025); Jeon et al. (2024), where generalization has been associated to the emergence of spurious states (Pham et al., 2025).

The connection between information theory and generative diffusion has motivated a growing body of work. As an example, Premkumar (2024) investigated entropy-based loss functions inspired by stochastic thermodynamics. Similarly, Kong et al. (2023a) and Kong et al. (2023b) reinterpreted several aspects of generative diffusion in an information theoretical framework. On a more applied side, recent work on discrete (Dieleman et al., 2022) and continuous diffusion (Stancevic et al., 2025) introduced the use of the conditional entropy function as a time-change for sampling and training diffusion models.

3 INFORMATION THEORY

We start by presenting an introduction to the information theory of sequential generative modeling, which will open the door to the analysis of generative diffusion.

Consider a game of *Twenty Questions* where an interrogator player may ask twenty binary questions concerning a set to an "oracle" player in order to gradually reveal the identity of a predetermined element \mathbf{y}^* in a finite set $\Omega = \{\mathbf{y}_1, \dots, \mathbf{y}_{N_0}\}$ with N_0 elements. We denote the size of the possible set $\Omega_{j-1}(a_{1:j-1})$ after $j-1$ questions as $N_{j-1}(a_{1:j-1})$. The answer a_j to the j -th question q_j then divides the set into two possible subsets with sizes $N_j^1(a_{1:j-1}) = N_j(a_j = 1, a_{1:j-1})$ and $N_j^0(a_{1:j-1}) = N_{j-1}(a_{1:j-1}) - N_j(a_j = 0, a_{1:j-1})$. Assuming a fixed set of questions, the expected uncertainty experienced by the player after the j -th question can be quantified by the conditional entropy:

$$H(\mathbf{y}^* | a_{1:j}) = -\mathbb{E}_{\mathbf{y}^*, a_{1:j}} [\log_2 p(\mathbf{y} | a_{1:j})] = \mathbb{E}_{a_{1:j}} [\log_2 N_j(a_{1:j})] \quad (1)$$

where \mathbf{y}^* is sampled uniformly from Ω . Under these conditions, the expected entropy reduction associated to a given question is given by

$$\Delta H_j = \mathbb{E}_{a_{1:j}} \left[\log_2 N_{j-1} - \frac{N_j^0}{N_{j-1}} \log_2 N_j^0 + \frac{N_j^1}{N_{j-1}} \log_2 N_j^1 \right], \quad (2)$$

where we left the dependence on the set of answers implicit to unclutter the notation. It is easy to see that the maximum bit rate is 1, which is achieved when $N_j^0 = N_{j-1}/2$. Assuming that 20 questions are enough to fully identify the value of \mathbf{y}^* , we can encode each \mathbf{y} in the string of binary values $a_{1:20}$, which makes clear that the question answering process consists of gradually filling in this string. Using the language of generative diffusion, we can re-frame this process in terms of a 'forward' process, where the string $a_{1:20}$ corresponding to an element of Ω is sampled in advance and then transmitted to the j -th 'time point' through the following non-injective forward process

$$R_j(a_{1:20}) = a_{1:j}, \quad (3)$$

which deterministically suppresses information by masking the values of the string. The solution of a Twenty Question game can then be seen as inverting this 'forward process'. Note that the forward process leads to a sequence of monotonically non-decreasing marginal conditional entropies $H(\mathbf{y}^* | a_{1:j}) < H(\mathbf{y}^* | a_{1:j-1})$, which is a fundamental feature of a forward process in diffusion models that captures the fact that information is lost by the forward transformation.

Now consider the case where a lazy oracle forgot to select a word in advance and decides instead to answer the questions at random under the probability determined by the sizes N_j^0 and N_j^1 , which we assume to be fixed given the questions. Strikingly, this reformulation does not make any observable difference from the point of view of the interrogator as each (randomly sampled) answer equally reduces the space of possible words and it results in the same entropy reduction, until a final guess

can be offered. Therefore, the game of Twenty Questions with a random oracle can be interpreted as a sequential generative process where the state at 'time' j is given by a binary string $a_{1:j}$ with Markov transition probabilities

$$p(a_{j+1} = 0 \mid a_{1:j}) = \frac{N_{j+1}^0(a_{1:j})}{N_j(a_{1:j})} \quad (4)$$

The conditional entropy rate ΔH_j determines how much information is transferred from 'time' j to the final generation.

As we shall see, the reverse diffusion process can be seen as analogous to this 'generative game' with the score function playing the part of the interrogator and the noise ϵ_t playing the role of the oracle. Like in the interrogator in the generative Twenty Questions game, the score function can reduce the information transfer by tilting the probabilities of the stochastic increments out of uniformity, which reduces the impact of the noise. This phenomenon is related to the divergence of the vector field induced by the score function, which causes amplification of small perturbations during the generative dynamics. We will also see that the phenomenon is connected to the branching of paths of fixed-points of the score and consequently to the phenomenon of generative phase transitions and spontaneous symmetry breaking (Raya & Ambrogioni, 2023).

3.1 SCORE-MATCHING GENERATIVE DIFFUSION MODELS

The sequential generation example outlined above is analogous to called masked diffusion models Lou et al. (2023); Sahoo et al. (2024). On the other hand, score-matching generative diffusion models are continuous-time sequential generative models where the forward process is given by a diffusion process such as

$$d\mathbf{x}_t = \nu(t) d\mathbf{W}_t, \quad (5)$$

which is initialized with the data source $p(\mathbf{x}_0) = \rho(\mathbf{y})$. Generation in score-matching diffusion consists of integrating the 'reverse equation' Song et al. (2021):

$$d\mathbf{x}_t = -\nu^2(t) \nabla \log p_t(\mathbf{x}_t) + \nu(t) d\mathbf{W}_t, \quad (6)$$

where, for notational simplicity, we restrict our attention to the forward process given in Eq. 5. Note that Eq. 6 must be integrated backward with initial condition determined by the stationary distribution of the forward process.

The fundamental mathematical object that determines the reverse dynamics is the score function, which in this case can be expressed as $\nabla \log p_t(\mathbf{x}_t) = \mathbb{E}_{\mathbf{y}|\mathbf{x}_t} \left[\frac{\mathbf{x}_t - \mathbf{y}}{\sigma^2(t)} \right]$, where $\sigma^2(t) = \int_0^t \nu^2(\tau) d\tau$ is the total variance of the noise at time t and the expectation is taken with respect of the conditional distribution $p(\mathbf{y} \mid \mathbf{x}_t) \propto p(\mathbf{x}_t \mid \mathbf{y})\rho(\mathbf{y})$. This expression can be further simplified by noticing that $\mathbf{x}_t = \mathbf{y} + \sigma(t)\mathbf{z}_t$:

$$\nabla \log p_t(\mathbf{x}_t) = -\mathbb{E}_{\mathbf{z}|\mathbf{x}_t} \left[\frac{\mathbf{z}}{\sigma(t)} \right] \quad (7)$$

where \mathbf{z} is a standard normal vector. In other words, the score is the negative of the average (rescaled) noise and it therefore provides the optimal (infinitesimal) denoising direction.

In dynamical term, the score function determines the vector field (i.e. the drift) that guides the generative paths towards the distribution of the data.

In practice, a normalized score network $s(\mathbf{x}_t; \theta)$ should be trained to minimize the rescaled score-matching loss:

$$\mathcal{L}_{\text{sm}}(\theta, t) = \mathbb{E}_{\mathbf{x}_t} \left[\|\sigma(t) \nabla \log p_t(\mathbf{x}_t) - s(\mathbf{x}_t; \theta)\|^2 \right] \quad (8)$$

This loss function cannot be computed directly because the true score is not available. However, Eq. 8 can be re-written using Eq. 7 and expanding the square:

$$\begin{aligned} \mathcal{L}_{\text{sm}}(\theta, t) &= \mathbb{E}_{\mathbf{x}_t} \left[\left\| \mathbb{E}_{\mathbf{z}|\mathbf{x}_t} [\mathbf{z}] - s(\mathbf{x}_t; \theta) \right\|^2 \right] \\ &= \mathbb{E}_{\mathbf{z}, \mathbf{y}} \left[\|\mathbf{z} - s(\mathbf{y} + \sigma(t)\mathbf{z}; \theta)\|^2 \right] - \mathbb{E}_{\mathbf{z}, \mathbf{y}} \left[\|\mathbf{z} - \sigma(t) \nabla \log p_t(\mathbf{y} + \sigma(t)\mathbf{z})\|^2 \right]. \end{aligned} \quad (9)$$

Note that the second term is constant in θ , which means that the gradient solely depends on the denoising loss:

$$\mathcal{L}_d(\theta, t) = \mathbb{E}_{\mathbf{z}, \mathbf{y}} \left[\|\mathbf{z} - s(\mathbf{y} + \sigma(t)\mathbf{z}; \theta)\|^2 \right]. \quad (10)$$

The constant term

$$C_t = \mathbb{E}_{\mathbf{z}, \mathbf{y}} \left[\|\mathbf{z} - \sigma(t)\nabla \log p_t(\mathbf{y} + \sigma(t)\mathbf{z})\|^2 \right] \quad (11)$$

is of high importance for our current purposes. It quantifies the loss of the denoiser obtained from the score function. This is therefore the unavoidable part of the denoising error that is still present given a perfectly trained network. With a few manipulations, it is possible to show that this term is in fact equal to the variance of the posterior denoising distribution:

$$C_t = \mathbb{E}_{\mathbf{y}, \mathbf{x}_t} [\text{var}(\mathbf{y} \mid \mathbf{x}_t)], \quad (12)$$

which allows us to interpret this term as a measure of uncertainty at time t on the final outcome of the generative trajectory.

4 GENERATIVE INFORMATION TRANSFER IN SCORE MATCHING DIFFUSION

To characterize the generative information transfer we need to compute the conditional entropy rate $\dot{H}(\mathbf{y} \mid \mathbf{x}_t)$, which is the analogous of the discrete entropy reduction we gave in Eq. 2. The conditional entropy is defined as

$$H(\mathbf{y} \mid \mathbf{x}_t) = -\mathbb{E}_{\mathbf{y}, \mathbf{x}_t} [\log p(\mathbf{y} \mid \mathbf{x}_t)] \quad (13)$$

To find the entropy rate, we can take the temporal derivative of Eq. 13 and use the Fokker-Planck equation, which in our case is just the heat equation:

$$\partial_t p_t(\mathbf{x}_t) = \frac{1}{2} \nu^2(t) \nabla^2 p_t(\mathbf{x}_t). \quad (14)$$

Using integration by parts, this results in

$$\begin{aligned} \dot{H}[\mathbf{y} \mid \mathbf{x}_t] &= \frac{\nu^2(t)}{2} \left(\mathbb{E}_{p(\mathbf{x}_t, \mathbf{x}_0)} [\|\nabla \log p(\mathbf{x}_t \mid \mathbf{x}_0)\|^2] - \mathbb{E}_{p_t(\mathbf{x}_t)} [\|\nabla \log p(\mathbf{x}_t)\|^2] \right) \\ &= \frac{\nu^2(t)}{2} \left(\frac{D}{\sigma^2(t)} - \mathbb{E}_{p_t(\mathbf{x}_t)} [\|\nabla \log p(\mathbf{x}_t)\|^2] \right), \end{aligned}$$

where D is the dimensionality of the ambient space. From this formula, we can see that the maximal bandwidth is reached when the euclidean norm of the score function is minimized.

To gain some insight on the significance of the square norm, consider the case where m data points $\mathbf{y}_1(\mathbf{x}_t) \dots \mathbf{y}_m(\mathbf{x}_t)$ have non-vanishing probability $p(\mathbf{y}_j \mid \mathbf{x}_t) = 1/m$ and that their differences from $\mathbf{y}_t(\mathbf{x}_t)$ have the same norm and are mutually orthogonal: $(\mathbf{y}_j(\mathbf{x}_t) - \mathbf{x}_t)^T (\mathbf{y}_k(\mathbf{x}_t) - \mathbf{x}_t) = \delta_{jk}^k \sigma_t^2$. The score function is an average under the posterior distribution $p(\mathbf{y} \mid \mathbf{x}_t)$, which in this case is given by

$$\nabla \log p_t(\mathbf{x}_t) = \mathbb{E}_{\mathbf{y} \sim p(\mathbf{y} \mid \mathbf{x}_t)} \left[\frac{(\mathbf{y} - \mathbf{x}_t)}{\sigma^2(t)} \right] \approx \frac{1}{m} \sum_{j=1}^m \frac{\mathbf{y}_j(\mathbf{x}_t) - \mathbf{x}_t}{\sigma_t^2}. \quad (15)$$

Due to our assumption of orthogonality of the differences, we have that, in this case, the expected squared norm of the score is given by

$$\mathbb{E}[\|\nabla \log p_t(\mathbf{x}_t)\|^2] \approx \frac{1}{m^2} \sum_{j=1}^m \mathbb{E}[\|\mathbf{y}_j(\mathbf{x}_t) - \mathbf{x}_t\|^2] / \sigma_t^4 = \frac{1}{\sigma_t^2 m}. \quad (16)$$

This implies that the norm is a decreasing function of the size m of the 'active set' of data points with non-negligible probability given \mathbf{x}_t . This is because the effect of several 'active datapoints' results in destructive interference (i.e. cancellation) in the average. This phenomenon allows us to interpret the length of the score vector as an estimate of uncertainty in the denoising process, with higher uncertainty being associated with a higher entropy rate (see Eq. 16). As we shall see in the rest of the paper, we can associate peaks in the entropy rates with symmetry-breaking bifurcations that correspond to noise-induced 'choices' between possible data points.

4.1 CONDITIONAL ENTROPY PRODUCTION AS OPTIMAL ERROR

The conditional entropy rate quantifies the instantaneous generative information transfer at any given moment in time. It can be shown (see (Stancevic et al., 2025)) that this quantity is closely connected to the optimal denoising squared error, which is the variance of the denoising distribution:

$$\dot{H}[\mathbf{y}|\mathbf{x}_t] = \frac{1}{2} \frac{\nu^2(t)}{\sigma^4(t)} \mathbb{E}_{\mathbf{y}, \mathbf{x}_t} [\text{var}(\mathbf{y} \mid \mathbf{x}_t)] . \quad (17)$$

Intuitively, this means that the information rate is directly related to the denoising uncertainty at a given time.

Using this relation, we can now re-express the denoising score matching formula in Eq. 9 in terms of the conditional entropy rate:

$$\mathbb{E}_{\mathbf{x}_t} \left[\left\| \mathbb{E}_{\mathbf{z} \mid \mathbf{x}_t} [\mathbf{z}] - s(\mathbf{x}_t; \theta) \right\|^2 \right] + \frac{2\sigma^4(t)}{\nu^2(t)} \dot{H}[\mathbf{y}|\mathbf{x}_t] = \mathbb{E}_{\mathbf{z}, \mathbf{y}} \left[\left\| \mathbf{z} - s(\mathbf{y} + \sigma(t)\mathbf{z}; \theta) \right\|^2 \right] , \quad (18)$$

which implies that the entropy rate can be estimated from the training loss if we assume that the network is well trained.

4.2 GENERATIVE BANDWIDTH

It is insightful to investigate under what situation the score-matching diffusion model can achieve the maximum possible generative bandwidth. From Eq. 15, it is clear that this happens when $\mathbb{E} [\|\nabla \log p_t(\mathbf{x}_t)\|] = 0$, which in turn is obtained if the score vanishes everywhere.

To realize this situation, we can consider a data distribution $p_h(\mathbf{y})$ to be a centered multivariate normal with variance h^2 . In this case, the score function is just:

$$\nabla \log p_t(\mathbf{x}_t) = -\frac{\mathbf{x}_t}{\sigma^2(t) + h^2} , \quad (19)$$

which vanishes everywhere for $h \rightarrow 0$, giving a maximum entropy rate:

$$\dot{H}(\mathbf{x}_0 \mid \mathbf{x}_t) = \frac{1}{2} \frac{D\nu^2(t)}{\sigma^2(t)} . \quad (20)$$

This corresponds to a setting where the particles are free to diffuse since every possible generation is equally likely. From this, we can conclude that the score function has the negative role of suppressing fluctuations along 'unwanted directions' to preserve the statistics of the data and that peaks in the information transfer comes from periods where noise fluctuations are not suppressed. Note that the maximum bandwidth scales with the dimensionality D .

Now consider the case where the distribution of the data is a centered Gaussian in a D_{data} -dimensional subspace with $D_{\text{data}} \leq D$. In this case, the expected norm of the score decomposes as follows

$$\mathbb{E} \left[\|\nabla \log p_t(\mathbf{x}_t)\|^2 \right] = \frac{D_{\text{data}}}{\sigma^2(t) + h^2} + \frac{D - D_{\text{data}}}{\sigma^2(t)} \rightarrow \frac{D - D_{\text{data}}}{\sigma^2(t)} \quad (21)$$

which leads to the entropy rate

$$\dot{H}(\mathbf{x}_0 \mid \mathbf{x}_t) = \frac{1}{2} \frac{D_{\text{data}}\nu^2(t)}{\sigma^2(t)} . \quad (22)$$

In this case, the score function suppresses entropy reduction in the subspace orthogonal to the data and therefore acts as a linear analog filter. Note that the entropy rate is zero when D_{data} is equal to zero since all the distribution is in this case collapsed into a single point and no 'decision' needs to be made.

5 STATISTICAL PHYSICS, ORDER PARAMETERS AND PHASE TRANSITIONS

In this section, we will connect the information theoretical concepts we outlined above with concepts from statistical physics such as order parameters, phase transitions and spontaneous symmetry breaking. We will start by studying the paths of fixed-points of the score function and use them to track 'generative decisions' (i.e. bifurcations) along the denoising trajectories. As we will see, the stability of these fixed-points paths is regulated by the Jacobian of the score and it is deeply connected with the conditional entropy production.

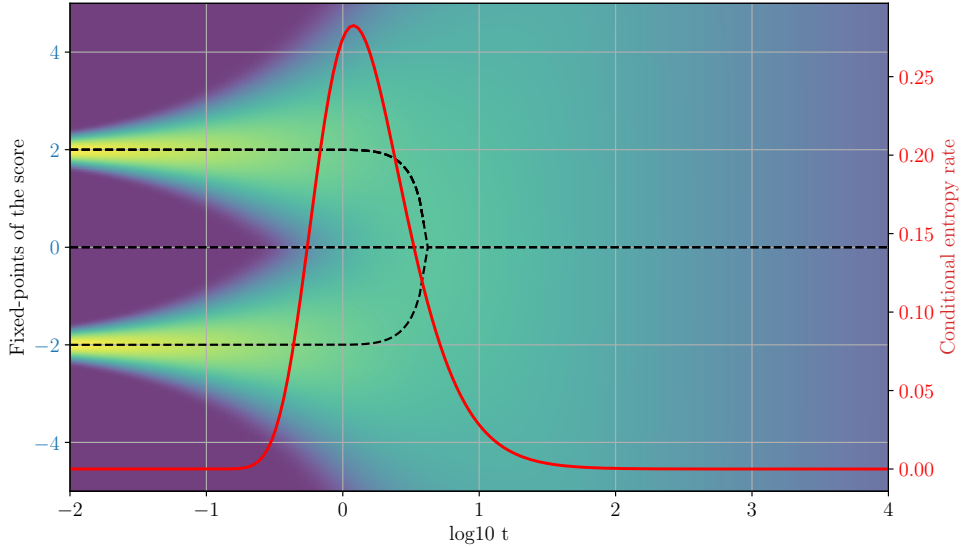


Figure 1: Conditional entropy profile (left) and paths of fixed-points (right) for a mixture of two delta distributions. The color in the background visualizes the (log)density of the process.

5.1 BRANCHING PATHS OF FIXED-POINTS AND SPONTANEOUS SYMMETRY BREAKING

The fixed-points of the score function are defined by the equation:

$$\nabla \log p_t(\mathbf{x}_t^*) = \mathbf{0} \quad (23)$$

We denote the set of fixed-points at time t as Ψ_t . The solutions of this fixed-point equation can be organized in a set Ω of piecewise continuous paths $\gamma : \mathbb{R}^+ \rightarrow \mathbb{R}^d \in \Omega$. To remove ambiguities, we assume that, if $\gamma(\tau)$ is discontinuous at τ_0 , then the one-sided limit exists and it is equal to $\lim_{t \rightarrow \tau^+} \gamma(\tau) = \arg \min_{\mathbf{x} \in \Psi_t} \|\mathbf{x} - \gamma(\tau)\|$. We know that $\lim_{t \rightarrow \infty} \gamma(t) = \mathbf{0}$ for all paths since the zero vector is the only fixed-point of the score of the asymptotic Gaussian distribution. Any two paths $\gamma_1(t)$ and $\gamma_2(t)$ can be proven to overlap for a finite range of time, meaning that $\gamma_1(t) = \gamma_2(t)$ if $t \geq \tau_{12} \in \mathbb{R}^+$ (this follows from the results in (Carreira-Perpinan, 2002; Carreira-Perpinan & Williams, 2003; Améndola et al., 2020) on the number of modes of mixture of normal distributions). We refer to $\tau_{1,2}$ as the *branching time* of the two paths. The branching time of two paths of fixed points can roughly be interpreted as a *decision time* in the generative process, where the sample will be ‘pushed’ by the noise in either one or the other path during the reverse dynamics. It is therefore insightful to study the behavior of the paths at the branching times. In general, this can happen if there is a discontinuous jump in a path $\gamma(t)$. Perhaps more interestingly, two paths can also branch continuously at a finite time. This can be studied by analyzing the Jacobian matrix of the score function:

$$J_t(\mathbf{x}_t^*) = \nabla^T \nabla \log p_t(\mathbf{x}_t^*) \quad (24)$$

. We say that a path $\gamma(t)$ is stable at time t if $J_t(\gamma(t))$ is negative-definite, and we say that the path is stable if this is true for all $t \in \mathbb{R}^+$ except for a countable set of time points t_j where the Jacobian is negative semi-definite. Now consider two stable paths $\gamma_1(t)$ and $\gamma_2(t)$ that branch continuously at time $\tau_{1,2}$. Given the asymptotic separation vector

$$\mathbf{v}_{1,2} = \lim_{t \rightarrow \tau_{1,2}^-} \frac{(\gamma_2(t) - \gamma_1(t))}{\|\gamma_2(t) - \gamma_1(t)\|},$$

it can be shown that $\mathbf{v}^T J_t(\gamma(t)) \mathbf{v} < 0$ in a finite interval $(\tau_{1,2}, \tau_{1,2} + \epsilon)$ and that

$$\lim_{t \rightarrow \tau_{1,2}^+} \mathbf{v}^T J_t(\gamma_1(t)) \mathbf{v} = 0,$$

which implies that the second directional derivative of $D_{\mathbf{v}}^2 \log p_t(\mathbf{x}_t)$ along \mathbf{v} vanishes at the branching point.

Consider now a generative diffusion with

$$p_0(\mathbf{y}) = \frac{1}{K} \sum_{j=1}^K \delta(\mathbf{y}^{(j)} - \mathbf{y}), \quad (25)$$

with K distinct data-points $\mathbf{y}^{(j)} \in \mathbb{R}^d$. In this case, there are exactly K distinct stable fixed-point paths $\gamma_j(t)$, with $\gamma_j(0) = \mathbf{y}^{(j)}$. Again, any two paths branch at a finite time $\tau_{j,k}$. For a given t , we can partition the set of data-points in equivalence classes, where two data-points $\mathbf{y}^{(j)}$ and $\mathbf{y}^{(k)}$ share the same class if their associated path coincide at t . Importantly, each equivalence class corresponds to an individual fixed-point, which allows us to associate each fixed-point $\mathbf{x}^* \in \Psi_t$ to a sub-set of data-points that are, using colorful language, fused together. More precisely, we can express the fixed-points as weighted averages of data-points obtained by solving the self-consistency equation:

$$\mathbf{x}^* = \sum_{j=1}^K w_j(\mathbf{x}^*) \mathbf{y}^{(j)} \quad (26)$$

where

$$w_j(\mathbf{x}) = \frac{e^{\left(\|\mathbf{y}^{(j)}\|^2/2 + \mathbf{x}^T \mathbf{y}^{(j)}\right)/\sigma^2(t)}}{\sum_{k=1}^K e^{\left(\|\mathbf{y}^{(k)}\|^2/2 + \mathbf{x}^T \mathbf{y}^{(k)}\right)/\sigma^2(t)}}. \quad (27)$$

Note that this average has non-zero weight on all data points, which is why we cannot find the location of the fixed-point solely based on its equivalence class. However, usually the weights corresponding to data-points in the equivalence class will be substantially larger than the other weights and will therefore dominate the average. In summary, we can interpret the set of fixed-points as a decision tree where each branching point roughly coincides with a split between two sets of data points.

An example of spontaneous symmetry breaking happens when the generative path needs to 'decide' between two isolated data-points. Consider again the mixture of delta case and two neighboring data-points $\mathbf{y}_1 = \mathbf{v}$ and $\mathbf{y}_2 = -\mathbf{v}$. If the distance between the center of mass of these two points and the nearest external data-point is much larger than $\sigma(t)$, there will be a fixed point approximately located along the line segment connecting the two points. In these conditions, we can consider the fixed-point equation restricted to the projections on \mathbf{v} :

$$x_v^* = \tanh\left(\frac{x_v^* + \phi(x_v^*, t)}{\sigma^2(t)}\right) \quad (28)$$

where $\phi(x_v^*, t)$ encapsulates the interference due to all other data-points, which we, in this example, we assume to be small relative to the norm of the separation vector:

$$\phi(x_v^*, t) = \frac{\sigma^2(t)}{2} \left(\log \left(e^{x_v^*} + \sum_{j \neq 1, 2}^K y_v^{(j)} e^{\left(-\|\mathbf{y}^{(j)}\|^2/2 + x_v y_v^{(j)}\right)/\sigma^2(t)} \right) - x_v^* \right).$$

If we approximate the interference function with constant ϕ using a zero-th order Taylor expansion, Eq. 28 becomes the self-consistency equation of a Curie-Weiss model of magnetism, with temperature $T = \sigma^2(t)$ and external magnetic field ϕ . The solutions of this equation can be visualized as intersection points between a straight line and a hyperbolic tangent (see (Ambrogioni, 2024b) and (Raya & Ambrogioni, 2023) for a detail analysis). When ϕ is finite, the system transitions discontinuously from one to two fixed-points, which corresponds to a first-order phase transition in the magnetic system. However, the size of the discontinuity vanishes when $\phi = 0$, when there is an exact symmetry between the two data-points (see Fig. 1). This gives rise to a so called *critical phase transition*, where a single fixed-point at $x^* = 0$ continuously splits into two paths $\mathbf{x}_1(t)$ and $\mathbf{x}_2(t)$ with $\mathbf{x}_{1,2}(t - t_c) \sim \pm(t - t_c)^{1/2}$ for $t \rightarrow 0$. The loss of stability of the fixed-point at the origin corresponds to the vanishing of the quadratic well around the point:

$$\frac{\partial^2}{\partial x_v^2} \log p_{t_c}(x_v^*) = 0 \quad (29)$$

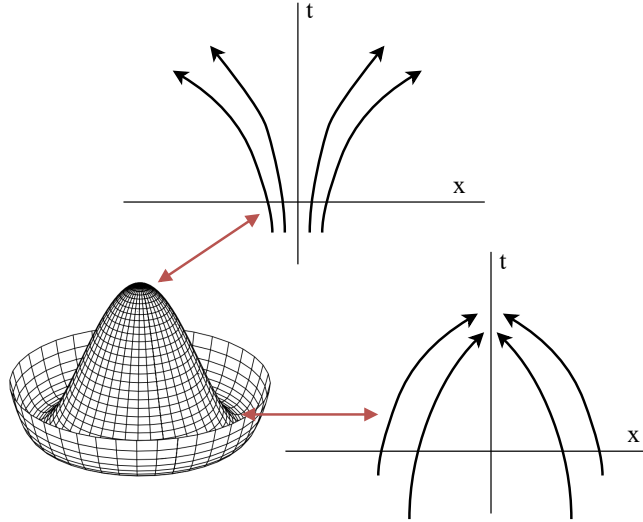


Figure 2: Stability and instability of trajectories in different parts of a symmetry-breaking potential. Generative branching is associated with divergent trajectories.

, where, in this case, $\mathbf{x}_{t_c}^* = 0$ for $t < t_c$. The analysis we just carried out involves the breaking of the permutation symmetry between two isolated data-points. On the other hand, if the symmetry is broken along all directions like in the case where the data manifold is a sphere centered at \mathbf{x}_t^* , Eq. 29 implies that

$$\text{Tr} [\nabla^T \nabla \log p_t(\mathbf{x}_{t_c}^*)] = \nabla \cdot \nabla \log p_t(\mathbf{x}_{t_c}^*) = \mathbf{0} \quad (30)$$

Therefore, the change in stability condition can be reformulated as the local vanishing (or suppression in a less symmetric case) of the divergence of the vector field that drives the generative dynamics. The transition from the super-critical ($t > t_c$) and the sub-critical ($t < t_c$) phases then corresponds to a sign change in the divergence of the vector field (i.e, the score) in the spherically-symmetric case, or a sign change of the divergence restricted to a sub-space in the general case, with the sub-critical regime being characterized by positive eigenvalues of the Jacobi matrix that lead to divergent local trajectories (see Fig. 2).

6 DYNAMICS OF THE GENERATIVE TRAJECTORIES

Around a point \mathbf{x}^* , the local behavior of the generative trajectories under the deterministic ODE flow dynamics can be characterized by its Lyapunov exponent, which quantifies the separation rate of infinitesimally close trajectories. In particular, the minimal local exponent for a perturbation along a unit vector \mathbf{w} , which in the reverse dynamics can be defined as

$$l_{\mathbf{w}}(t, \mathbf{x}) = \lim_{\tau \rightarrow \infty} \lim_{\mathbf{w} \rightarrow 0} \frac{1}{\tau} \log \frac{\|\mathbf{x}_{t-\tau}(\mathbf{x}_t + \mathbf{w}) - \mathbf{x}_{t-\tau}(\mathbf{x}_t)\|}{\|\mathbf{w}\|}, \quad (31)$$

where $\mathbf{x}_{t-\tau}(\mathbf{x}_t + \mathbf{w})$ denotes a deterministic generative trajectory with the perturbed initial condition. Note that in reality τ cannot tend to infinity in the generative dynamics since time is only defined up to 0. However, we will still consider this limit since we are only interested in the local asymptotic behavior of the linearized dynamics around a bifurcation point. Under the reverse dynamics, when the Lyapunov exponent along \mathbf{w} is negative, infinitesimal perturbations are amplified exponentially (at least locally) by the generative dynamics.

We can use the notion of minimal local Lyapunov exponent to formalize the phenomenon of local divergence of trajectories after a spontaneous symmetry breaking event at t_c . To study the local sub-critical behavior, we consider the linearization of the dynamics around the unstable fixed point

for $t < t_c$ and $t_c - t = \epsilon$:

$$l_{\mathbf{w}}(t_c + \epsilon, \mathbf{x}) = \lim_{\tau \rightarrow \infty} \lim_{\mathbf{w} \rightarrow \mathbf{0}} \frac{1}{\tau} \log \frac{\left\| e^{-\tau J_{t_c - \epsilon}(\mathbf{x}_{t_c - \epsilon}^*)} \mathbf{w} \right\|}{\|\mathbf{w}\|} = \lambda_{\min}(\mathbf{x}_{t_c - \epsilon}^*, t_c + \epsilon), \quad (32)$$

where $\lambda_{\min}(\mathbf{x}_{t_c - \epsilon}^*, t_c + \epsilon)$ is the smallest of the eigenvalues of the Jacobi matrix whose eigenvectors overlap with \mathbf{w} . In the immediate sub-critical phase of a symmetry breaking phase transition, we know that there is a non-empty sub-space spanned by the eigenvector of the Jacobian corresponding to negative eigenvalues. Therefore, perturbations along this unstable eigen-space will be exponentially amplified by the generative dynamics. In the stochastic case, this can be seen as a critical 'macroscopic amplification' of the infinitesimal noise input, where the noise breaks the symmetry of the generative model. In the deterministic dynamics, the symmetry is instead broken by the amplification of small differences between the generative trajectories.

In general, we will refer to the spectrum of Jacobian eigenvalues $\lambda_j(\mathbf{x}_t, t)$ as the local Lyapunov spectrum. As we shall see, this spectrum can be directly related to the conditional entropy production.

6.1 THE GLOBAL PERSPECTIVE ON GENERATIVE BIFURCATIONS

In the previous sections, we characterized the generative dynamics of diffusion models by studying the associated paths of fixed-points in term of their stability and bifurcations, which led us to establish formal connections with the statistical physics of phase transitions and symmetry breaking. However, in high dimension, small volumes around a fixed-point have vanishingly low probability of being visited. In fact, due to the dispersive effect of the noise, the generative trajectories are concentrated on fixed-variance shells around the fixed points. More formally, these set of "typical" points form tabular neighborhoods of the set of fixed-points (see 1). It is therefore unclear how a bifurcation in a path of fixed-points affects the behavior of the generative trajectories, since the analysis we presented in the previous sections was purely local.

To gain insight into the global behavior of the typical generative trajectories, we can study the expected divergence of the vector field

$$\text{div}(t) = \mathbb{E}_{\mathbf{x}_t} [\nabla \cdot \nabla \log p_t(\mathbf{x}_t)] = \mathbb{E}_{\mathbf{x}_t} [\text{Tr} [\nabla^T \nabla \log p_t(\mathbf{x}_t)]] . \quad (33)$$

If $\text{div}(\mathbf{x}_t)$ is negative, the separation between the generative trajectories will on average be contracted by the generative dynamics. The simplest example of this contractive behavior can be studied by considering a data distribution with a single point: $p_0(\mathbf{x}_t) = \delta(\mathbf{y} - \mathbf{c})$. In this case, all trajectories converge to \mathbf{c} for $t \rightarrow 0$, and we have

$$\text{div}_1(t) = -\frac{D}{\sigma^2(t)} . \quad (34)$$

where D is the dimensionality of the space. In the reverse dynamics, the negative sign implies that the forward process produces a stable dynamics where the particles 'fall' towards the data points.

In the general case, this quantity can be identified with the "trivial component" of the expected divergence since it does not depend on the data but only on the forward process. In the general case, it can be expressed as

$$\text{div}_1(t) = \mathbb{E}_{\mathbf{x}_t} [\text{Tr} [\nabla^T \nabla \log p_t(\mathbf{x}_t \mid \mathbf{y})]] . \quad (35)$$

We can therefore study the purely data-dependent part of the expected divergence by subtracting this "trivial component":

$$\Delta \text{div}(t) = \text{div}(t) - \text{div}_1(t) . \quad (36)$$

Intuitively, $\Delta \text{div}(\mathbf{x}_t)$ encodes the separation of the typical trajectories in the reverse process due to bifurcations in the generative process, which mirrors the local analysis we carried out in the previous sections at the level of the fixed-points.

Using integration by parts, it is straightforward to connect the expected divergence with the conditional entropy rate

$$\dot{H}[\mathbf{y} \mid \mathbf{x}_t] = \frac{\nu^2(t)}{2} \Delta \text{div}(t) \quad (37)$$

Therefore, the expected data-dependent divergence of the generative trajectories directly determines the conditional entropy rate. From this identity, we can immediately deduce that $\Delta \text{div}(\mathbf{x}_t)$ is non-negative valued and consequently that $\text{div}(t) \geq \text{div}_1(t)$.

We can also show that the marginal entropy is produced by the expected divergence

$$\dot{H}[\mathbf{x}_t] = -\frac{\nu^2(t)}{2} \text{div}(t), \quad (38)$$

which implies that $\text{div}(t) \leq 0$ since the marginal entropy is a monotonically increasing function of t under our forward process. This reflects the fact that the forward process always lead to a dispersion of the trajectories, regardless to the nature of the initial distribution. From this, we can conclude that the maximum bandwidth is achieved when

$$\text{div}(t) = \mathbb{E}_{\mathbf{x}_t} [\text{Tr} [\nabla^T \nabla \log p_t(\mathbf{x}_t)]] \rightarrow 0. \quad (39)$$

This gives us a clear connection between the local vanishing of the Jacobian in spontaneous symmetry breaking (Eq. 30) with the expected vanishing that corresponds to saturation of the generative bandwidth.

6.2 INFORMATION GEOMETRY

The derivation in the previous sub-section suggests a deep connection between the information production and the geometry of the data manifold. We can further analyze this connection by using concepts from information geometry Amari (2016). The key connection is that conditional entropy rate is in fact just the expected value of the trace of the Fisher information matrix, which can be defined as follows:

$$\mathcal{I}_t(\mathbf{x}_t) = -\mathbb{E}_{\mathbf{y}|\mathbf{x}_t} [\nabla \nabla^T \log p(\mathbf{y} | \mathbf{x}_t)]. \quad (40)$$

This quantity quantifies the sensitivity of the posterior distribution $p(\mathbf{y} | \mathbf{x}_t)$ to changes in \mathbf{x}_t and can be interpreted as a natural metric tensor on the variable \mathbf{x}_t . Using Bayes theorem and our simplified forward process, the expression can be rewritten as

$$\mathcal{I}_t(\mathbf{x}_t) = \sigma^{-2}(t) (I + \sigma^2(t) J(\mathbf{x}_t)), \quad (41)$$

Geometric information such as the manifold dimensionality is encoded in the spectrum of this matrix Kadkhodaie et al. (2023); Stanczuk et al. (2024); Ventura et al. (2024); Achilli et al. (2025). The Fisher information metric provides information on the (local) manifold structure of the data \mathbf{y} as seen through the lenses of the noisy state \mathbf{x}_t . This is easy to see in the case where the data is Gaussian with covariance matrix Σ_0 , which gives the formula

$$\mathcal{I}_t = \sigma^{-2}(t) I - (\Sigma_0 + \sigma^2(t) I)^{-1}. \quad (42)$$

When \mathbf{y} is supported on a D_{data} manifold, the (degenerate) eigenvalue λ_{\parallel} corresponding to the orthogonal complement is equal to zero. On the other hand, in the flat limit, the tangent eigenvalues become equal to Σ_0^{-1} . This implies that the dimensionality of the manifold is given by the dimensionality of the eigenspace corresponding to the eigenvalue $\lambda_{\parallel} = \sigma^{-2}(t)$. In the general case, the eigen-decomposition of $\mathcal{I}(\mathbf{x}_t)$ characterizes the local tangent structure of the manifold Stanczuk et al. (2024); Ventura et al. (2024).

We can now use these expressions to cast light on the geometry of entropy production. The conditional entropy rate is directly related to the trace of the Fisher information matrix:

$$\dot{H}(\mathbf{y} | \mathbf{x}_t) = \frac{1}{4} \nu^2(t) \mathbb{E}_{\mathbf{x}_t} [\text{Tr}[\mathcal{I}(\mathbf{x}_t)]], \quad (43)$$

which reduces to Eq. 22 in the linear manifold case we just considered. From this perspective, it is clear that the reduction in bandwidth is the result of the suppression of the eigenvalues of $\mathcal{I}(\mathbf{x}_t)$. This can also be seen in the general case by re-expressing the entropy rate in terms of the expected eigenvalues of the Jacobi matrix:

$$\dot{H}(\mathbf{y} | \mathbf{x}_t) = \frac{\nu^2(t)}{4\sigma^2(t)} \left(D + \sigma^2(t) \sum_j \mathbb{E} [\lambda_j(\mathbf{x}_t)] \right). \quad (44)$$

This equation shows that the entropy production is directly regulated by the spectrum of expected local Lyapunov exponents, as studied in our local analysis.

We can better understand this formula by re-writing it as follows:

$$\dot{H}(\mathbf{y} \mid \mathbf{x}_t) = \frac{\nu^2(t)}{4} \sum_j (1/\sigma^2(t) + \mathbb{E} [\lambda_j(\mathbf{x}_t)]) . \quad (45)$$

From this, we can see that conditional entropy production in a eigenspace is fully suppressed when $\mathbb{E} [\lambda_j(\mathbf{x}_t)] = -1/\sigma^2(t)$, which is the eigenvalue of the Jacobian of the conditional score under the isotropic forward process.

7 A THERMODYNAMIC PERSPECTIVE

A deeper insight on the processes being conditional entropy production can be gained by studying the temporal evolution of the marginal entropy, which is just the thermodynamic entropy of the system. As we discussed above, conditional entropy production corresponds to expected divergence of trajectories in the reverse process, or equivalently to expected convergence of trajectories in the forward process. An interesting way to see this is by considering the identity

$$\dot{H}[x_t] = -\frac{\nu^2(t)}{2} (\text{div}_1 + \Delta \text{div}(t)) = \frac{D\nu^2(t)}{2\sigma^2(t)} - \dot{H}(\mathbf{y} \mid \mathbf{x}_t) \quad (46)$$

The first term of this expression is always positive and leads to the monotonic decrease in entropy during the reverse process. Perhaps more interesting is the role of the conditional entropy in the formula. Since the conditional entropy is always non-negative, $-\dot{H}(\mathbf{y} \mid \mathbf{x}_t)$ is either negative or zero. This implies that the conditional entropy rate, if we ignore the other forward term, produces a paradoxical increase of thermodynamic entropy during the reverse process. This paradoxical entropy production is the result of what we referred to as 'generative decisions'. In reality this entropy production is always compensated by the forward term, so that the 'second law' is never violated and the generative decisions correspond to decreases in entropy reduction during the reverse process.

8 DISCUSSION & CONCLUSIONS

This paper has presented a unified framework that connects the dynamics, information theory, and statistical physics of generative diffusion. We have shown that the generative process is governed by the conditional entropy rate, which is directly tied to the expected divergence of the score function's vector field. This divergence drives the branching of generative trajectories, which we characterize as symmetry-breaking phase transitions. By analyzing the fixed-points of the score function and their stability, we demonstrate that the model's sequential decisions during generation are formalized as noise-induced bifurcations, mapping directly onto mean-field models like the Curie-Weiss magnet.

In conclusion, generative diffusion can be understood as a dynamical system that progressively breaks symmetries in the energy landscape. The flow of information is modulated by the score function, which suppresses noise in irrelevant directions while allowing critical fluctuations to drive the system between possible outcomes. This synthesis provides a foundation for understanding how these models transform noise into structured data, offering a new perspective that connects the learning dynamics of modern generative AI to fundamental concepts in statistical physics. This framework opens avenues for designing more efficient models and analyzing their generalization behavior. The connection between phase transitions and training dynamics can lead to improved sampling and training schedules that explicitly target critical periods of high information transfer (see (Stancic et al., 2025) for a preliminary work in this direction). Furthermore, our formalism provides a natural tool for rigorously studying memorization, mode collapse, and generalization challenges often described heuristically—by analyzing the stability and topology of the learned score function's fixed-points. Finally, these insights may guide the development of novel model classes that more explicitly incorporate hierarchical and semantic structure through controlled symmetry breaking.

REFERENCES

Beatrice Achilli, Enrico Ventura, Gianluigi Silvestri, Bao Pham, Gabriel Raya, Dmitry Krotov, Carlo Lucibello, and Luca Ambrogioni. Losing dimensions: Geometric memorization in generative diffusion. *arXiv preprint arXiv:2410.08727*, 2024.

Beatrice Achilli, Luca Ambrogioni, Carlo Lucibello, Marc Mézard, and Enrico Ventura. Memorization and generalization in generative diffusion under the manifold hypothesis. *Journal of Statistical Mechanics: Theory and Experiment*, 2025(7):073401, 2025.

Ahmed El Alaoui, Andrea Montanari, and Mark Sellke. Sampling from mean-field gibbs measures via diffusion processes. *arXiv preprint arXiv:2310.08912*, 2023.

Shun-ichi Amari. *Information Geometry and Its Applications*, volume 194. Springer, 2016.

Luca Ambrogioni. In search of dispersed memories: Generative diffusion models are associative memory networks. *Entropy*, 26(5):381, 2024a.

Luca Ambrogioni. The statistical thermodynamics of generative diffusion models: Phase transitions, symmetry breaking and critical instability. *arXiv preprint arXiv:2310.17467*, 2024b.

Carlos Améndola, Alexander Engström, and Christian Haase. Maximum number of modes of gaussian mixtures. *Information and Inference: A Journal of the IMA*, 9(3):587–600, 2020.

Joe Benton, Valentin De Bortoli, Arnaud Doucet, and George Deligiannidis. Nearly d-linear convergence bounds for diffusion models via stochastic localization. In *International Conference on Learning Representations*, 2024.

Giulio Biroli and Marc Mézard. Generative diffusion in very large dimensions. *Journal of Statistical Mechanics: Theory and Experiment*, 2023(9):093402, 2023.

Giulio Biroli, Tony Bonnaire, Valentin de Bortoli, and Marc Mézard. Dynamical regimes of diffusion models. *Nature Communications*, 15(1), 2024. doi: 10.1038/s41467-024-54281-3.

Tony Bonnaire, Raphaël Urfin, Giulio Biroli, and Marc Mézard. Why diffusion models don't memorize: The role of implicit dynamical regularization in training. *arXiv preprint arXiv:2505.17638*, 2025.

Miguel A. Carreira-Perpinan. Mode-finding for mixtures of gaussian distributions. *IEEE Transactions on Pattern Analysis and Machine Intelligence*, 22(11):1318–1323, 2002.

Miguel A Carreira-Perpinán and Christopher KI Williams. On the number of modes of a gaussian mixture. In *International Conference on Scale-Space Theories in Computer Vision*, 2003.

Prafulla Dhariwal and Alex Nichol. Diffusion models beat GANs on image synthesis. *arXiv preprint arXiv:2105.05233*, 2021.

Sander Dieleman, Laurent Sartran, Arman Roshannai, Nikolay Savinov, Yaroslav Ganin, Pierre H. Richemond, Arnaud Doucet, Robin Strudel, Chris Dyer, Conor Durkan, et al. Continuous diffusion for categorical data. *arXiv preprint arXiv:2211.15089*, 2022.

Joshua Hess and Quaid Morris. Associative memory and generative diffusion in the zero-noise limit. *arXiv preprint arXiv:2506.05178*, 2025.

Jonathan Ho, Ajay Jain, and Pieter Abbeel. Denoising diffusion probabilistic models. *Advances in Neural Information Processing Systems*, 33:6840–6851, 2020.

Benjamin Hoover, Hendrik Strobelt, Dmitry Krotov, Judy Hoffman, Zsolt Kira, and Duen Horng Chau. Memory in plain sight: A survey of the uncanny resemblances between diffusion models and associative memories, 2023. *Associative Memory & Hopfield Networks* in 2023.

Bai Huang, Andrea Montanari, and Huy Tuan Pham. Sampling from spherical spin glasses in total variation via algorithmic stochastic localization. *arXiv preprint arXiv:2404.15651*, 2024.

Dongjae Jeon, Dueun Kim, and Albert No. Understanding memorization in generative models via sharpness in probability landscapes. *arXiv preprint arXiv:2412.04140*, 2024.

Zahra Kadkhodaie, Florentin Guth, Eero P Simoncelli, and Stéphane Mallat. Generalization in diffusion models arises from geometry-adaptive harmonic representations. *arXiv preprint arXiv:2310.02557*, 2023.

Xianghao Kong, Rob Brekelmans, and Greg Ver Steeg. Information-theoretic diffusion. *arXiv preprint arXiv:2302.03792*, 2023a.

Xianghao Kong, Ollie Liu, Han Li, Dani Yogatama, and Greg Ver Steeg. Interpretable diffusion via information decomposition. *arXiv preprint arXiv:2310.07972*, 2023b.

Aaron Lou, Chenlin Meng, and Stefano Ermon. Discrete diffusion language modeling by estimating the ratios of the data distribution. *arXiv preprint arXiv:2305.14627*, 2023.

Andrea Montanari. Sampling, diffusions, and stochastic localization. *arXiv preprint arXiv:2305.10690*, 2023.

Bao Pham, Gabriel Raya, Matteo Negri, Mohammed J. Zaki, Luca Ambrogioni, and Dmitry Krotov. Memorization to generalization: Emergence of diffusion models from associative memory. *arXiv preprint arXiv:2505.21777*, 2025.

Akhil Premkumar. Neural entropy. *arXiv preprint arXiv:2409.03817*, 2024.

Gabriel Raya and Luca Ambrogioni. Spontaneous symmetry breaking in generative diffusion models. *arXiv preprint arXiv:2305.19693*, 2023.

Robin Rombach, Andreas Blattmann, Dominik Lorenz, Patrick Esser, and Björn Ommer. High-resolution image synthesis with latent diffusion models. *arXiv preprint arXiv:2112.10752*, 2022.

Subham Sahoo, Marianne Arriola, Yair Schiff, Aaron Gokaslan, Edgar Marroquin, Justin Chiu, Alexander Rush, and Volodymyr Kuleshov. Simple and effective masked diffusion language models. *Advances in Neural Information Processing Systems*, 37:130136–130184, 2024.

Antonio Sclocchi, Alessandro Favero, Noam Itzhak Levi, and Matthieu Wyart. Probing the latent hierarchical structure of data via diffusion models. *Journal of Statistical Mechanics: Theory and Experiment*, 2025(8):084005, 2025a.

Antonio Sclocchi, Alessandro Favero, and Matthieu Wyart. A phase transition in diffusion models reveals the hierarchical nature of data. *Proceedings of the National Academy of Sciences*, 122(1): e2408799121, 2025b.

Jascha Sohl-Dickstein, Eric A. Weiss, Niru Maheswaranathan, and Surya Ganguli. Deep unsupervised learning using nonequilibrium thermodynamics. *arXiv preprint arXiv:1503.03585*, 2015.

Jiaming Song, Chenlin Meng, and Stefano Ermon. Denoising diffusion implicit models. *arXiv preprint arXiv:2010.02502*, 2022.

Yang Song, Jascha Sohl-Dickstein, Diederik P. Kingma, Abhishek Kumar, Stefano Ermon, and Ben Poole. Score-based generative modeling through stochastic differential equations. *arXiv preprint arXiv:2011.13456*, 2021.

Dejan Stancevic, Florian Handke, and Luca Ambrogioni. Entropic time schedulers for generative diffusion models. *arXiv preprint arXiv:2504.13612*, 2025.

Jan Paweł Stanczuk, Georgios Batzolis, Teo Deveney, and Carola-Bibiane Schönlieb. Diffusion models encode the intrinsic dimension of data manifolds. In *International Conference on Machine Learning*, 2024.

Enrico Ventura, Beatrice Achilli, Gianluigi Silvestri, Carlo Lucibello, and Luca Ambrogioni. Manifolds, random matrices and spectral gaps: The geometric phases of generative diffusion. *arXiv preprint arXiv:2410.05898*, 2024.